Influence of Supramolecular Interaction Type on Photoresponsive Azopolymer Complexes: A Surface Relief Grating Formation Study

Xin Wang,[a,b] Jaana Vapaavuori,[b] Xiaoxiao Wang,[b] Ribal Georges Sabat,[c]

Christian Pellerin,[b] C. Geraldine Bazuin*,[b]

[a] School of Materials Science and Engineering, Southwest Petroleum University, Chengdu, China 610500

[b] Département de chimie, Centre de recherche sur les matériaux auto–assemblés (CRMAA/CSACS), Université de Montréal, C.P. 6128, succursale Centre-Ville, Montréal (QC), Canada H3C 3J7

[c] Department of Physics, Royal Military College of Canada, Kingston (ON), Canada K7K 7B4

* Email: geraldine.bazuin@umontreal.ca

TOC graphic:

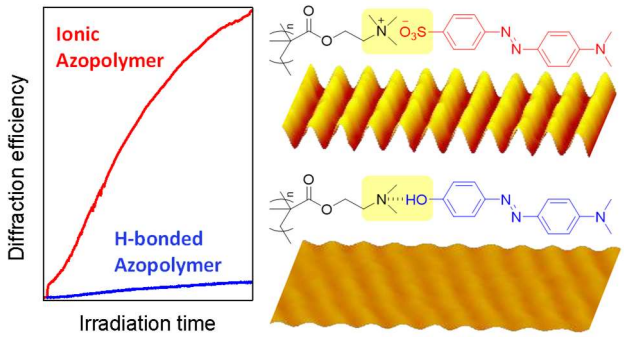

ABSTRACT. The influence of the supramolecular interaction type – hydrogen bonding, proton transfer and pure ionic bonding – on photoresponsive behavior, particularly surface relief grating (SRG) inscription, has been investigated using a homopolymer with an ambient temperature glass transition (T_g). To this end, poly(dimethylaminoethyl methacrylate) (PDMAEMA or PDM) of relatively high molecular weight (42k) was complexed at various azo/DM molar ratios with dimethylamino azobenzene derivatives functionalized by hydroxyl (azoOH) or carboxylic acid (*p*-methyl red or azoCOOH) groups, and quaternized PDM (PDMQ) was complexed at equimolar ratio with a sulfonated analog (methyl orange or azoSO_3), and the structural and thermal properties of these complexes were determined. SRG inscription on spin-coated films was found to be possible because complexation increases the T_g above ambient. The efficiency of SRG inscription on spin-coated films, which increases with azo content, is highest for the purely ionic azoSO_3/PDMQ complex despite its very high T_g, while the proton transfer azoCOOH/PDM complexes, involving ionic and H-bonding with acid-salt structures, show somewhat more efficient SRG inscription than do the purely hydrogen-bonded azoOH/PDM complexes, and this despite some azoCOOH crystallization at the highest molar ratios. These findings clarify the comparative effectiveness of different supramolecular bond types on SRG inscription and provide a useful guide for the design of supramolecular photoresponsive polymers for SRG applications.

INTRODUCTION

Azobenzene motifs, which undergo trans-cis photoisomerization under irradiation of light in the UV-visible region, are widely used in photoresponsive materials.[1,2] These materials have a variety of potential applications, some of them based on the formation of surface relief gratings or SRGs. Photoinduced SRGs are inscribed in photoresponsive films by exposure to an interference pattern of light whose wavelength lies in the absorption band of the azo group, causing directional polymer chain motion on a macroscopic scale,[1,3-5] a phenomenon that has given rise to an alternative term, directional photofluidization lithography, to describe SRG inscription.[6] Because the periodicity, amplitude and form of the gratings can be controlled by the optical setup, SRGs can be exploited in areas such as photonics, either by using SRGs directly or as micro- and nanopatterning templates for diffraction gratings, antireflection coatings, light-polarization converters and plasmonic sensors.[7]

Although much research has been conducted on SRG formation with many different materials, the mechanism underlying it and the various material parameters that influence it are still not well understood.[2,6,8,9] To reach a better experimental understanding as well as to design easily tailorable new materials, several groups in recent years have turned to a supramolecular strategy, where appropriately functionalized azo-containing small molecules are non-covalently bonded to passive polymers possessing complementary groups.[10-27] This approach greatly facilitates the preparation of series of photoresponsive materials where specific material parameters can be varied systematically. Among the parameters that are crucial in designing supramolecular materials is the type of interaction, which, for SRG studies, has included hydrogen,[10-16] ionic[17-22] and halogen[23-25] bonding. A number of these have been shown to lead to efficient SRG formation, but almost no direct comparisons between the different interaction types or strengths on SRG formation have been made, excepting analogous hydrogen- and halogen-bonding materials.[23-25] For these, it was found that halogen bonding leads to more efficient SRG formation compared to hydrogen bonding,[23-25] which was attributed to greater directionality and hence

molecular linearity[23,24] and to the absence of plasticization effects[25] in the halogen-bonded systems. Many of the supramolecular systems used in SRG investigations to date are based on polymers having relatively high glass transition temperatures (T_g), especially poly(4-vinyl pyridine) (P4VP)[10,13,14,20,23,26] and sometimes polyphenol.[12,27] For the former, complexes were typically made by simple mixing of the polymer with OH- or COOH-functionalized azo molecules, whereas for the latter pyridine-functionalized azo molecules were appropriate. These all lead to hydrogen-bonded complexes, albeit with different strengths.

In the above context, SRG formation in supramolecular complexes based on poly(dimethylaminoethyl methacrylate) (PDM) is of interest. Due to the more basic character of the tertiary amine in PDM compared to pyridine in P4VP, the nature of PDM bonding with OH- and COOH-functionalized azo molecules is fundamentally different, notably pure hydrogen bonding for the former and a form of ionic bonding through proton transfer (but also involving H-bonding and acid-salt structures, as explained later) for the latter, allowing a direct comparison of these two bonding types. It will be shown that, although the T_g of PDM itself is low (near ambient), which can negatively affect the temporal stability of the SRGs, complexation increases the T_g to thereby enable SRG inscription. On the other hand, it has generally been considered that very high T_g's inhibit efficient SRG inscription, although this is not supported by our previous results for ionic complexes based mainly on quaternized P4VP ion-exchanged with sulfonated azo molecules where the influence of the molecular flexibility on photoinduced birefringence and SRG formation was determined.[20] Since PDM can also be quaternized and ion-exchanged to obtain a high-T_g complex characterized by pure ionic bonding,[20] it is a simple matter to directly compare SRG inscription using this ionic complex with the hydrogen-bonded and proton-transfer complexes.

Thus, the aim of the present work is to characterize the three types of complexes shown in Scheme 1, where the azo molecules in each case are identical except for the functional group forming the complex

with PDM, and to compare the SRG inscription on films of these complexes in relation to their properties. The complexes are referred to hereafter as azoCOOH/PDM(y), azoOH/PDM(y) and azoSO_3/PDMQ(1.0), where y refers to the molar ratio of the azo molecule to polymer repeat unit (DM or DMQ), which is varied for the azoOH and azoCOOH complexes and equimolar only for the azoSO_3 complex. They will sometimes be referred to collectively as azoSM (SM for small molecule).

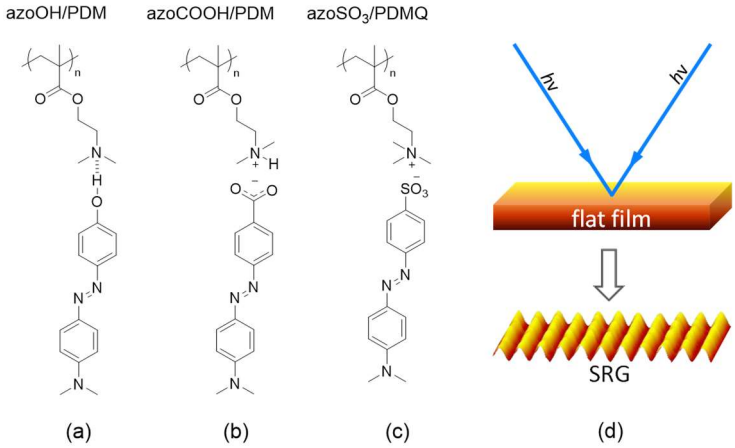

Scheme 1. Targeted azo-containing complexes self-assembled from (a) azoOH, (b) azoCOOH or (c) azoSO_3 and the polymer, poly(dimethylaminoethyl methacrylate) (PDM; PDMQ when quaternized). The effect of three types of interactions on surface relief grating (SRG) formation is compared: (a) pure hydrogen bonding, (b) proton transfer leading to mixed ionic and hydrogen bonding, and (c) pure ionic bonding via ion exchange. AzoSM/DM molar ratios vary between 0.1 and 1.0 for (a) and (b), and are 1.0 only for (c). A simple schematic of SRG inscription is shown in (d).

EXPERIMENTAL

Materials. All materials were obtained from Sigma-Aldrich unless otherwise specified. 4-Hydroxy-4'-dimethylaminoazobenzene (azoOH, >98.0%, Tokyo Chemical Industry), 4-dimethylaminoazobenzene-4'-carboxylic acid (azoCOOH, also called *p*-methyl red, >97.0%, Tokyo Chemical Industry), sodium 4-[(4-dimethylamino)phenylazo]benzenesulfonate (azoSO_3Na, also called methyl orange), aluminum oxide (Al_2O_3, activated neutral), ethylene bis(2-bromoisobutyrate), *N,N,N′,N′,N*-pentamethyldiethylenetriamine (PMDETA, 99%), anhydrous anisole (99.7%), anhydrous

DMF (99.8%), DMSO (ACS grade, American Chemical), THF (HPLC grade, Fisher Scientific), hexane (ACS grade, Fisher Scientific), nitromethane (ACS grade, J. T. Baker), iodomethane (99.5%), and triethylamine (≥99.0%) were all used as received. *N,N'*–dimethylaminoethyl methacrylate (DMAEMA or DM, 98%) was passed through a neutral Al_2O_3 column just before polymerization to eliminate the inhibitor. Copper (I) bromide (CuBr, 98%) was washed with boiling acetic acid before use to remove any soluble oxidized species. Deionized water was obtained from a Millipore Gradient A10 Milli-Q system.

Instrumentation. The molecular weight and polydispersity of PDM were measured at room temperature by size exclusion chromatography coupled with quasi-elastic light scattering (SEC-LS), using a Wyatt QELS system equipped with a Waters 600E pump, two PLgel 300×7.5 mm columns with a particle size of 5 μm and pore sizes of 10^3 Å and 10^5 Å, respectively, a refractive index detector and a photodiode array detector. THF with 2 vol % triethylamine (TEA) was used as the eluent, the flow rate was 1 mL/min, and the solution concentration was about 3 mg/mL. Freeze-drying was effected using a FTS Systems FD-3-85A-MP freeze-dryer working at 1-3 mT with the condenser at -90 °C. Spin-coating was done at 3000 rpm for 30 s at room temperature using a Headway Research EC101D instrument. The thicknesses of the spin-coated films on glass slides were measured using a Bruker DektakXT profilometer with Vision64 software across a scratch made close to the inscribed SRG using a bamboo toothpick dipped in DMF.

^{1}H NMR spectra were recorded on a Bruker Avance spectrometer (400 MHz). Energy dispersive spectrometric (EDS) analysis was done using a FEI Quanta 200 FEG environmental scanning electron microscope equipped with an energy dispersive spectrometer. Fourier transform infrared (IR) spectra in transmission mode were recorded using a Thermo Scientific Nicolet spectrometer. Those in ATR (attenuated total reflection) mode were recorded using a Tensor 27 spectrometer (Bruker Optics) equipped with a HgCdTe detector and a MIRacle (Pike Technologies) ATR accessory with a silicon

element. The spectra were obtained with a resolution of 4 cm^{-1} by averaging 200 scans. UV-visible spectra were recorded using an Agilent Cary Series UV-vis-NIR spectrophotometer.

Surface relief grating inscription was achieved by guiding a circularly polarized beam of an Ar^+ laser, operating at a wavelength of 488 nm and an irradiance of 50 or 190 mW/cm^2 (referred to hereafter as lower and higher irradiance, respectively), to a Lloyd's mirror interferometer for producing an interference pattern incident to the thin film of the sample, leading to SRG periodicities of 750 and 790 nm for inscription at lower and higher irradiance, respectively. SRG inscription was monitored by measuring the first-order diffraction of a 633-nm HeNe laser recorded by a photodiode. The gratings were maintained in ambient conditions for 1 and 2 days for inscription at lower and higher irradiance, respectively, before being stored in a vacuum oven at room temperature. They were imaged by tapping mode atomic force microscopy (AFM) under ambient atmosphere using a Digital Instruments (Bruker) Multimode microscope, a Nanoscope V controller, Nanoscope V7.30 software and Nanoworld tips (Arrows NC model, spring constant 42 N/m, oscillation frequency 285 kHz, tip radius <10 nm).

Differential scanning calorimetry (DSC) of 3-9 mg of samples placed in standard aluminum DSC pans was performed at heating and cooling rates of 10 °C/min using a TA Instruments Q2000 DSC. Wide angle X-ray diffraction (WAXD) analysis on solid power-like samples in glass capillaries (O.D. 1.0 mm, length 80 mm, thickness 0.01 mm, Charles Supper) was performed with a Bruker Microstar X-ray system operated at 45 kV and 20 mA using Cu Kα radiation at a sample-to-detector distance of 50 mm. The temperature was controlled by an Oxford cryosystem. The acquisition time for each sample was 60 s. Small angle X-ray scattering (SAXS) of the azoSO_3/PDMQ sample in the glass capillary was performed at room temperature at a sample-to-detector distance of 107.15 cm using a Bruker NanoStar X-ray instrument equipped with a Bruker Vantec-2000 area detector, a 50 kW 600-μA generator, an Incoatec IμS copper X-ray radiation source with a high-flux pinhole configuration, and a vacuum sample chamber at a pressure below 0.2 mbar. Grazing incidence wide-angle X-ray diffraction (GIWAXD) at an incidence

angle of 0.2° was conducted at room temperature on spin-coated films (the same as used for SRG, thus with similar thicknesses and on glass slides) with this same instrument at a sample-to-detector distance of 15 cm. Polarizing optical microscopy (POM) observations of these films were made at room temperature using a Zeiss Axioskop2 Plus microscope with a Plan Neofluar 40x/0.85 lens.

Synthesis and basic characterization of PDM and azoSM/PDM complexes. The PDM homopolymer was synthesized by atom transfer radical polymerization (ATRP) following a literature procedure.[28,29] Briefly, the polymerization was carried out in anhydrous anisole at 50 °C at an initiator/catalyst/monomer molar ratio of 1/1/380, where the initiator is ethylene bis(2-bromoisobutyrate) and the catalyst is CuBr/PMDETA. The product was purified by precipitating twice in hexane, drying under vacuum at room temperature for at least two days, and then storing in a desiccator containing drierite. The molecular weight, M_n, and the polydispersity were determined by SEC-LS to be 41.8 kg/mol and 1.38, respectively. The refractive index curve showed unimodal distribution. The relatively high polydispersity can be attributed to the amine function in DM that competes weakly with the ligand to coordinate with the copper catalyst, reducing it to inactive Cu(II), as observed also for ATRP of 4-vinylpyridine.[30]

The components for the azoCOOH/PDM and azoOH/PDM complexes were dissolved separately in anhydrous DMF (100 mg/mL for PDM, 50 mg/mL for azoOH, and 10 mg/mL for azoCOOH, the solubility of azoCOOH in DMF being more limited than that of azoOH). Then, appropriate quantities of azoSM solutions were added to fixed quantities of PDM solutions in vials to obtain the targeted molar ratios. After the vials were closed and sealed with parafilm, the solutions, which were transparent, were shaken for 12 h at room temperature, and then stored in a drierite-filled desiccator until further use (such as for drop-casting or spin-coating; see later). An equimolar complex of azoSO_3Na and quaternized PDM (PDMQ) was also prepared, using an ion exchange procedure described previously,[20] where PDM was fully quaternized by iodomethane to give PDMQ, then complexed with azoSO_3Na in DMSO, followed

by dialysis in Milli-Q water to eliminate the Na^+ and I^- counterions and excess azoSO_3Na (initially in 1.1 eq relative to DMQ), freeze-drying for two days and vacuum-drying at 80 °C for another 2 days. Successful elimination of the Na^+ and I^- counterions was verified by their absence in EDS analysis.

The stoichiometries of all of the complexes were verified by solution NMR in DMF-d_7 (Figure S1 and Table S1 in the Supporting Information) and found to be within 10% of the target values. It was also verified that the drying procedures used did not cause any significant loss of the most weakly bonded small molecule, azoOH. This is shown, first, by the NMR spectra of the 0.10 and 1.0 complexes vacuum-dried at 50 ºC for 2 days, then stored under vacuum at room temperature for about two months (Table S1). Second, the IR spectra of the same complexes vacuum-dried at 50 °C for 2, 5 and 10 days show excellent superposition for the former and at most very minor loss of azoOH for the latter (Figure S2). The temperature of 50 °C was chosen for this analysis, since it was the typical temperature used for drying of the complexes.

Sample preparation. Samples for NMR verification were prepared by adding 650 μL of DMF-d_7 to 70 μL of complex solution. Solid powder-like samples for DSC, ATR-IR, WAXD and SAXS measurements were prepared by casting the DMF solutions of the complexes onto clean glass slides (VWR), followed by vacuum drying at 50 °C for 2 d (unless otherwise specified). The solids were then carefully removed from the slides using a razor, and stored under vacuum at room temperature until further use. Transmission IR spectra of the pure azoSM were obtained from pressed pellets of sample ground with KBr powder.

Spin-coated films from DMF solutions were prepared on appropriate substrates, either glass slides (cleaned with acetone and Kimwipes, and dried with compressed air) for UV-visible and SRG investigations or KBr windows (ø25×4 mm thick, Pike Technologies) for transmission IR analysis, followed by vacuum drying at 50 °C for 2 d. The solutions used to spin-coat films for the UV-visible measurements were diluted 2-5 times compared to those used to spin-coat films for the IR and SRG

experiments. The same films used for SRG were also used for GIWAXD and POM analysis. To obtain sufficiently thick films of the azoCOOH/PDM complexes for the SRG experiments (the azoCOOH/PDM solutions being more dilute than the azoOH/PDM solutions due to the lesser solubility of azoCOOH), the glass slides were heated slightly – more for the higher molar ratios – using a heat gun just prior to placing a drop of solution for spin-coating.

RESULTS AND DISCUSSION

The objective of the present work is to compare the formation of surface relief gratings (SRGs) on spin-coated films of three types of supramolecular complexes based on a low-T_g polymer. Before presenting these results, it is necessary to verify the nature and extent of complexation between the polymer and the azoSM in these films, as well as to determine their relevant properties and characteristics, particularly the molecular structure and T_g's, in order to rationalize the SRG results.

Spectroscopic characterization of the azoOH and azoCOOH complexes. UV-visible spectra can give useful information regarding the dispersion of the azo molecules in solid films, which is an indirect indicator of complexation. These spectra for spin-coated films of the azoOH and azoCOOH complexes on glass are shown in Figure 1 (A and B), in comparison with the pure azos in dilute DMF solution. The principal band in the spectra is assigned to the π-π* absorption of the trans isomer on which is superposed the n-π* absorption in the form of a shoulder at roughly 470 nm.[20,31,32] The blue shift of the π-π* absorption maximum of dilute azoOH in DMF compared to that of azoCOOH can be attributed to the larger dipole moment of the azoCOOH compared to the azoOH. This leads to greater separation from the n-π* band, which is therefore more visible for the azoOH complexes (and pure azoOH in solution[26]) than for the azoCOOH complexes. The arrows in Figure 1, which specify the laser wavelength used for SRG inscription, indicate that the inscription is effected in the n-π* absorption region, which leads to fast trans-cis-trans cycling as opposed to an accumulation of cis isomers under irradiation.

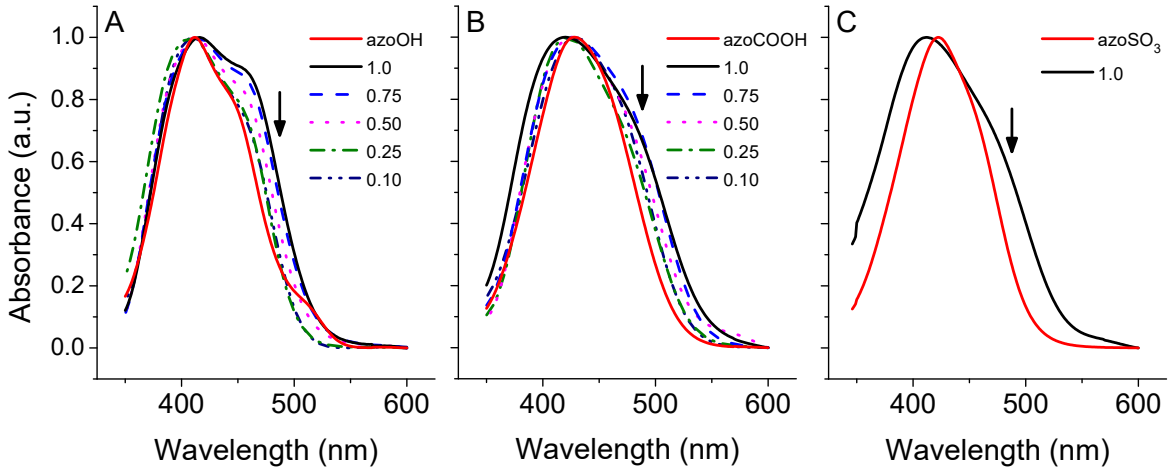

Figure 1. UV-visible absorption spectra of spin-coated films of (A) azoOH/PDM, (B) azoCOOH/PDM and (C) azoSO_3/PDMQ complexes at the molar ratios indicated, compared to the spectra of the pure azo molecules in dilute DMF solution (0.01, 0.01 and 0.04 mg/mL, respectively). The absorbance maxima were normalized to 1. The arrows identify the wavelength at which the SRGs were inscribed.

The similarity of the thin film spectra with the corresponding dilute solution spectra for the azoOH and azoCOOH systems implies that these azoSM are well dispersed in the films in all cases. For the azoOH series (Figure 1A), the maxima in the UV-visible spectra all lie at 412(±4) nm, with no systematic composition-dependent shift apparent. For comparison, the maximum for azoOH hydrogen-bonded to P4VP at various molar ratios in films spin-coated from DMF is also in this range (415 nm) and was considered indicative of unaggregated (i.e. non-crystallized) azoOH,[26] similarly to other examples in the literature for hydrogen-bonded complexes.[13,33,34] For the azoCOOH series (Figure 1B), the maximum of all but the 1.0 complex lies at 425(±3) nm, again indicative of essentially unaggregated azo, as found also for a closely-related COOH-functionalized azoSM (with a methylamino instead of dimethylamino tail) complexed by hydrogen-bonding to P4VP in equimolar ratio (in this case, the maximum lies at 433 nm, like the DMF solution spectra of both the complex and the pure azo).[10] For the 1.0 complex, there is a small blue shift (maximum at 420 nm), which is consistent with a low fraction of

aggregated or crystallized azoCOOH. Thus, assuming that unaggregated (non-crystallized) azoSM corresponds to PDM-complexed azoSM, the UV-visible data indicate that the azoSM are almost completely complexed to PDM in the spin-coated films except for equimolar azoCOOH/PDM for which there appears to be partial azoCOOH crystallization.

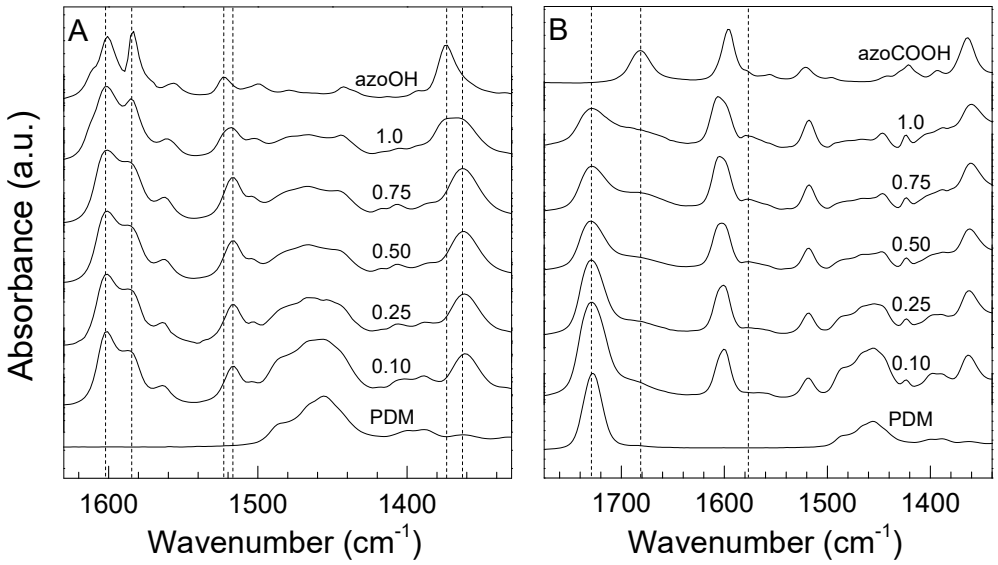

Figure 2. Ambient temperature infrared spectra of (A) azoOH/PDM and (B) azoCOOH/PDM complexes spin-coated on KBr windows at the azo/polymer molar ratios indicated, in comparison to those of the pure spin-coated PDM and pure azoSM in KBr pellets.

The nature and extent of interaction between supramolecular components, especially those involving hydrogen bonding and proton transfer interactions, can often be probed more directly using infrared spectroscopy. In the case of the present complexes between PDM and azoOH or azoCOOH, only qualitative, albeit still useful, information can be obtained by this method, as explained in what follows. IR spectra of samples spin-coated onto KBr windows are given in a selected spectral region in Figure 2 (complete spectra in Figures S3 and S4). The analyses are complicated by the fact that the pure azoSMs are crystalline with very high melting points (200 °C for azoOH;[35] simultaneous with degradation at about 230 °C, as measured by a melting point apparatus, for azoCOOH), but are dispersed (i.e.

amorphous) when complexed, which itself can modify intensities, widths and/or positions of various absorption bands. This along with overlapping of several PDM and azoSM bands and the weakness of tertiary amine bands, obscures changes caused by intercomponent interactions.

For the azoOH-containing films, various spectral shifts in location and intensity as a function of molar ratio are observed. Three bands or pairs of bands, shown in Figure 2A, are particularly noteworthy. First, the relative intensities of the pair of aromatic ring/phenol-related bands at about 1600 and 1585 cm^{-1} are not the same in the complexes compared to pure (crystalline) azoOH, despite the absence of PDM absorption in this region. Second, a band at 1373 cm^{-1} in the spectrum of pure azoOH (a mode involving most of the azo molecule, according to DFT calculations) shifts to 1362 cm^{-1} for the complexes with $y \leq 0.75$, while the 1.0 complex shows both components. Similarly, the band at 1523 cm^{-1} for pure azoOH shifts to 1516 cm^{-1} for the complexes with $y \leq 0.75$ and again shows both components for the 1.0 complex. These various spectral changes could be caused by phenol-amine H-bonding between azoOH and PDM, but may also simply be due to the amorphous nature of azoOH when dispersed in PDM in contrast to its crystalline state when pure.

To establish the origin of the observed spectral changes, infrared spectra in chloroform of pure azoOH and of a 1.0 molar ratio of azoOH mixed with a model tertiary amine, triethylamine (TEA), were taken. Figure S5 shows that the change in the intensity ratio of the 1600 and 1585 cm^{-1} bands is mainly due to dispersion since it is reproduced in the spectrum of pure azoOH in chloroform. In contrast, the 1523 cm^{-1} band is almost unaffected by azoOH dissolution in chloroform (it blue shifts by 1 cm^{-1}), but it red shifts to 1517 cm^{-1} in the presence of TEA, very similar to its position in the PDM complexes, thereby establishing that formation of azoOH-PDM hydrogen bonding takes place in the polymer complexes. Finally, the band at 1373 cm^{-1} is affected by both dispersion (leading to a maximum at 1369 cm^{-1} in chloroform) and hydrogen bonding (leading to a further shift to 1365 cm^{-1} in the presence of TEA). Our

results thus indicate essentially complete azoOH complexation up to at least 0.75 molar ratio, with only the 1.0 molar ratio sample containing some uncomplexed azoOH.

The result for the 1.0 complex appears to contrast somewhat with what was indicated by the UV-visible spectrum, which gives no clear evidence of azo crystallization. This might be related to the fact that the solutions used to prepare the films for UV-visible analysis were diluted in order to obtain thinner spin-coated films (to avoid saturation of the spectra). These thinner films likely lead to faster solvent evaporation and therefore less opportunity for aggregation/crystallization, or the substrate may impede azo crystallization in very thin films, which may depend also on its nature (glass vs. KBr). Furthermore, IR, with its much narrower absorption bands than UV-visible, is more sensitive to small amounts of crystallization. In addition, for a sample showing some tendency to crystallize, the degree of crystallinity is generally sensitive to the exact sample preparation conditions.

Regarding the azoCOOH-containing films (Figure 2B), for which proton transfer interactions from the acid to the PDM amino group are expected (the pKa of PDM is about 7.5[36]), the intense acid carbonyl band at 1681 cm^{-1} in the spectrum of pure azoCOOH, related to acid dimerization, is replaced in the spectra of the spin-coated azoCOOH/PDM complexes by a low-intensity broad absorbance in the same region (appearing as a shoulder on the low wavenumber side of the intense PDM ester carbonyl band at 1728 cm^{-1}). This is consistent with the conversion of a large fraction of acid carbonyl groups to carboxylate groups caused by proton transfer and indicative of a high extent of complexation. However, the low intensity or lack of clarity of asymmetric and symmetric carboxylate vibrations, which are typically found in the mid-to-high 1500 cm^{-1} region (a weak band is visible at about 1580 cm^{-1} in the complexes) and low-to-mid 1400 cm^{-1} region (obscured by another azoCOOH band and a broad PDM band), respectively,[37, 38] can be associated with the formation of acid-salt structures.[38-42] Such structures were encountered, for example, in blends of poly(acrylic acid) and a tertiary amine-functionalized surfactomesogen.[42-44] Acid-salt structures are, of course, a form of complexation, but their presence

implies that the nature of the complexation is not well defined and likely involves ionic and hydrogen bonding in possibly variable local structures that may also vary among samples, depending on precise details of sample preparation.[38,42] Other evidence for azoCOOH-PDM proton transfer interactions is given by the weak broad peaks at about 2450 and 2600 cm^{-1} (Figure S4), which may be related to (hydrogen-bonded) protonated tertiary amine absorption.[42] Although the extent of complexation cannot be quantified due to the complexity of the interactions, the changes in the infrared spectra, particularly the drastic reduction in the azoCOOH carbonyl band in the complexes, do suggest that it is high.

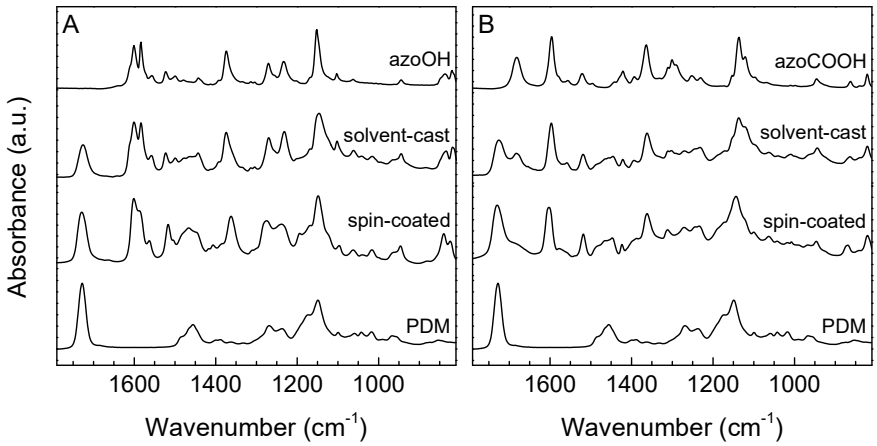

Figure 3. Infrared spectra of solvent-cast powder and spin-coated films of (A) azoOH/PDM(0.50) and (B) azoCOOH/PDM(0.50), in comparison with the pure components (ground with KBr for the azoSM and spin-coated for PDM).

As will be shown in the next section, solvent-cast complexes show much more azoSM crystallization than spin-coated films. This also allows a direct comparison of the IR spectra for complexes of the same composition that have two drastically different extents of crystallization and therefore complexation, as illustrated in Figure 3 for y=0.5. It can be observed that the spectra of the solvent-cast samples are much more similar to the additive spectra of the pure (crystallized) azoSM and pure PDM compared to the spectra of the spin-coated films. In particular, for the solvent-cast azoOH complex, the band at 1585 cm^{-1} is well-defined and has similar intensity to the 1600 cm^{-1} band and the

bands at 1523 and 1373 cm^{-1} are not shifted from their positions in pure azoOH, in contrast to the spin-coated film. Similarly, the 1681 cm^{-1} acid carbonyl band of the azoCOOH is much more intense and better defined in the spectrum of the solvent-cast sample than in the spectrum of the spin-coated film, whereas the (weak) 1578 cm^{-1} band attributed to the asymmetric carboxylate stretch and detectable in the spectrum of the spin-coated film is not present in the spectrum of the solvent-cast sample. This comparison demonstrates the sensitivity of IR to azoSM phase separation/crystallization and emphasizes the high level of complexation in the spin-coated azoSM/PDM films.

Structural and thermal characterization of the azoOH and azoCOOH complexes. Conventional structural and thermal analyses using X-ray diffraction (XRD) and DSC are generally not possible on spin-coated films, due to their being too thin to give sufficient signal. Therefore, for these latter analyses, solvent-cast samples were first prepared, giving thicker films that can be relatively easily recuperated for powder-type analyses. However, WAXD data for these samples (see Figure S6A, B) indicated significant azoSM crystallization in the azoOH complexes with molar ratios of 0.5 and greater (compared to none for 0.25 and 0.10) and in the azoCOOH complexes for all molar ratios (albeit weakly for 0.10). As indicated by the spectroscopic data above (and shown by XRD below), azoSM phase separation/crystallization is largely avoided in the spin-coated films. On the other hand, it was found that when the spin-coated films are dried at 70 °C (instead of the usual 50 °C), similar crystallization as in the solvent-cast samples occurs; i.e., for azoOH complexes, crystallization appeared for molar ratios of 0.75 and 1.0, whereas for azoCOOH complexes, it appeared for all of the molar ratios studied. Thus, both the film preparation method and the drying temperature can result in azoSM phase separation/crystallization, and this is more pronounced for the azoCOOH complexes than for the azoOH complexes. This will be further discussed in the last part of this section.

To obtain information regarding the state of crystallization in the spin-coated films, as used for the SRG investigations, grazing incidence wide-angle X-ray diffraction (GIWAXD) was employed. First,

for validation, it was applied to a spin-coated 1.0 azoOH/PDM film of about 0.9 μm thickness that was intentionally crystallized by holding it at 80 °C for 12 h (Figure 4A, top curve). This clearly demonstrated that the major crystalline reflections are detectable and comparable to a conventional WAXD diffractogram (see Figure S7). With this assurance, the technique was applied to all of the spin-coated films, as shown in Figure 4. The azoOH/PDM films all appear to be essentially amorphous, judging from the essentially featureless wide-angle halo in the diffractograms. For the azoCOOH/PDM films, there is clearly some crystallinity in the 1.0 sample, whereas a slight amount is detectable for the 0.25 to 0.75 molar ratios, and none in the 0.10 azoCOOH/PDM.

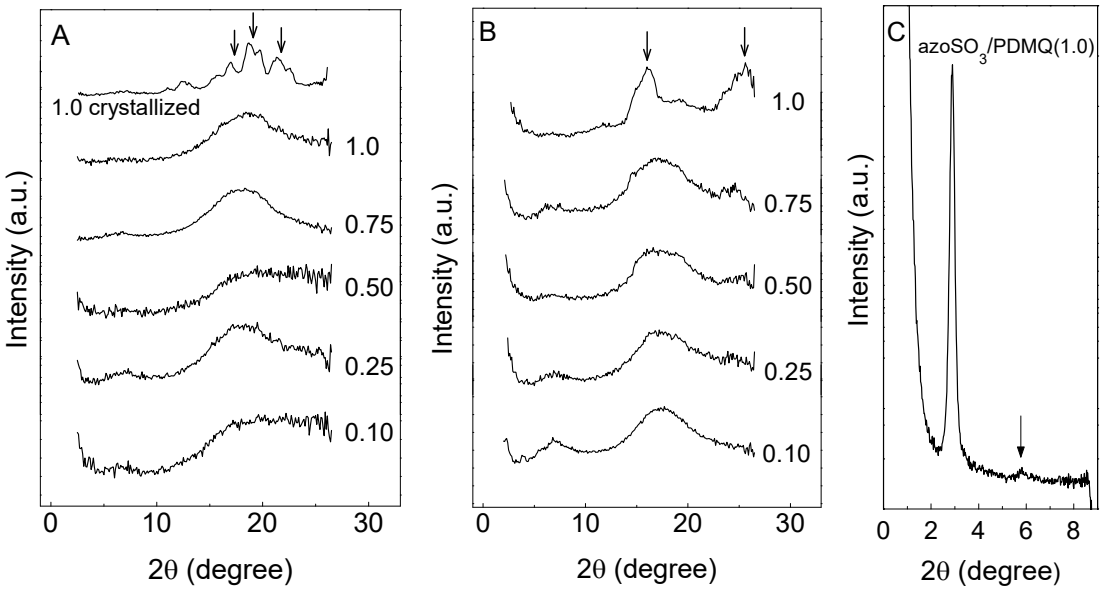

Figure 4. GIWAXD diffractograms of spin-coated films of (A) azoOH/PDM and (B) azoCOOH/PDM complexes, with an intentionally crystallized sample of 1.0 azoOH/PDM shown for comparison; the arrows point to some of the peaks indicative of crystallinity. (C) SAXS curve of the azoSO_3/PDMQ complex (solvent-cast powder), with arrow pointing to the second-order peak.

For further corroboration, polarizing optical microscopy (POM) images of the same spin-coated films (Figure S8) were obtained. These images show spots of birefringence for the azoCOOH/PDM films that are dense in the 1.0 sample, dispersed and more isolated in the 0.75 and 0.50 samples, almost absent

in the 0.25 sample, and totally absent in the 0.10 sample. They are also essentially absent in all of the azoOH/PDM films. Assuming that the birefringent spots arise from (sufficiently large) crystallites in the samples, the trends observed clearly parallel the GIWAXD trends. They are also similar to the IR data on the spin-coated films, although the IR data suggest a little more crystallization; in particular, the azoOH/PDM(1.0) complex shows partial crystallization according to IR, but none is clearly evident in the GIWAXD or POM data. This can be rationalized by the fact that IR can detect crystallites that are much smaller than are detectable by POM or GIWAXD (in addition to possible effects of detailed sample preparation and substrate effects, as mentioned earlier).

Given the low T_g of PDM and considering that the glass transition temperature is an important parameter for SRG formation and stability,[45] it is desirable to know how the T_g varies in the complexes. It was not possible, however, to determine a T_g on spin-coated films using DSC (it was attempted with a film spin-coated on Al foil, which was then cut into small circular pieces that were piled to maximum capacity in a DSC pan, but to no avail). On the other hand, it is possible to obtain useful information from DSC analysis of the solvent-cast samples (Figure S9). In particular, for the azoOH/PDM complexes (Figure S9A), the T_g, which is clearly defined for y=0.10, 0.25 and 0.50, is observed to increase with increasing azo content from about 30 to 55 to 80 °C, compared to the pure PDM T_g of 20 °C (Figure S9C). For y=0.10 and 0.25, the T_g's in the spin-coated films are probably very close to those in the solvent-cast samples, since WAXD of these samples indicates no crystallinity; even the T_g for the 0.50 solvent-cast sample may be only a little lower than in the spin-coated film, given the low crystallinity indicated by WAXD. For y=0.75, the T_g in the solvent-cast sample appears to be much higher, at about 120 °C, although it is very broad, and for y=1.0, it is about 90 °C, but these must be influenced by the presence of significant crystallinity. In the spin-coated films, where the degree of complexation is presumably complete or close to complete for all molar ratios as analyzed above, it can be expected that the T_g continues to increase with azoOH/DM molar ratio up to equimolar.

In comparison, the solvent-cast azoCOOH complexes (Figure S9B) have T_g's that are constant at about 25 °C for y=0.1-0.5, followed by an increase to about 55 °C for y=0.75 (again over a broad region) and then a decrease to about 35 °C for y=1.0. This is consistent with the maximum degree of complexation being close to 0.1, as indicated above, and implies that it stays constant near this ratio for the three lowest molar ratio complexes. If this is so, then it is unreasonable that the complexation can suddenly increase for y=0.75. Instead, it is speculated that the drastic increase in T_g for this molar ratio compared to lower molar ratios for both azoSM complexes might be related to an effective crosslinking effect of a critical number of uncomplexed nanoscale azo aggregates (e.g. nanocrystallites) that are also physically linked to the polymer chains via interfacial interactions with complexed azo and/or to reduced segmental mobility in the vicinity of those aggregates. The lower T_g for y=1.0 might then be related to larger but fewer azo aggregates that cannot as significantly affect the segmental mobility. Evidently, for the solvent-cast azoCOOH complexes, unlike for the solvent-cast azoOH complexes, DSC analysis does not provide useful information for the spin-coated films. However, based on the data and conclusions reached for the azoOH complexes and given that the GIWAXD and POM data for the spin-coated azoCOOH complex films indicates very limited crystallization up to y=0.75, which also imples that the degree of complexation in the spin-coated films must increase with azoCOOH content up to at least y=0.75, it is reasonable to assume that the T_g in the spin-coated azoCOOH films should show an increase with molar ratio, like for the azoOH films, up to at least y=0.75.

It is of interest to compare these results with P4VP-based systems with hydrogen-bonding azoSMs. For an OH-functionalized azo with a nitro tail, the T_g was also observed to increase with increasing azo content from 78 °C for y=0.05 to 105 °C for y=1.0 (P4VP MW=50k),[46] compared to about 140 °C for P4VP of relatively high molecular weight, whereas no particular tendency was noted for OH-functionalized azo molecules with a CN tail (the T_g's were stated to be between 60 and 80 °C; P4VP MW=50k);[26] moreover, in a system with an OH-functionalized bisazo molecule (Disperse Yellow 7), the

T_g was observed to decrease with increasing azo content from 125 °C for pure P4VP (MW=5400) to 60 °C for an equimolar complex.[13] Although the tendency with azo content appears to vary from system to system (noting that these T_g's were determined on samples prepared by slow solvent evaporation from solution), the T_g's of the complexes are always below the T_g of pure P4VP, in contrast to what is observed for the PDM systems here. Thus, the general T_g range for the azoSM/PDM complexes is roughly similar to that for analogous azoSM/P4VP complexes, attributed to the complexed azoSM having an overall chain rigidifying effect on low-T_g PDM and a plasticizing effect on high-T_g P4VP. The increase in T_g with increase in azoSM-PDM complexation is thus explained by the increased density of the relatively rigid azo molecules as effective side groups that expand the polymer chains and decrease their flexibility. For P4VP, this effect is counterbalanced by overall plasticization, which can be greater or less depending on the degree of rigidity/flexibility, degree of complexation, and type of packing of the azo molecule, so that the net effect as a function of azo content depends on the particular system, as noted above.

With knowledge of the T_g's, the observations above regarding azoSM crystallization can now be further discussed. First, the difference in azoSM crystallinity between the two film preparation methods can be attributed to the longer time required for solvent (DMF) evaporation from the thicker solvent-cast films compared to the thinner spin-coated films. In the latter, the evaporation is so rapid that, in most cases, molecular immobility (where the T_g presumably exceeds the operation temperature) sets in more quickly than (significant) phase separation/crystallization of the azo molecules can occur. The system is then frozen in, so that nearly dry films that are otherwise prone to azo crystallization (all of the azoCOOH/PDM complexes and the higher molar ratio azoOH/PDM complexes) remain stable during drying at 50 °C as well as during long-term storage at room temperature, indicating that the T_g's of those complexes are sufficiently high. The lower T_g of 30 °C measured for azoOH/PDM(0.10) [and 55 °C for azoOH/PDM(0.25)], which could in principle allow crystallization during drying at 50 °C, indicates that the H-bonding azo/polymer interactions are more favorable than azoOH crystallization. This is supported

by the observation that no crystallization in these two complexes was observed in any of the conditions applied, including solvent-casting. For the lowest molar ratio azoCOOH/PDM complexes, which show crystallization in the solvent-cast samples and which presumably also have relatively low T_g's (although they could be higher than for the azoOH/PDM complexes of the same molar ratio), it seems that the driving force for azoCOOH crystallization is not great enough to result in crystallization at 50 °C, probably due both to the low azoCOOH content and to high viscosity when still quite close to the T_g. In contrast, this is evidently no longer the case for drying at 70 °C, where azo crystallization that approaches that observed in the solvent-cast films takes place.

The greater tendency for crystallization in the azoCOOH complexes compared to the azoOH complexes is explained by the greater driving force related to the (relatively strong) acid dimerization interactions. Comparable behavior was reported in the literature for similar systems. In one example, phase separation and crystallization was noted in complexes of hydrogen-bonded azoSMs and P4VP-containing block copolymers during solvent annealing (by 1,4-dioxane vapor) of spin-coated films,[47] solvent annealing also reducing the system T_g and thereby greatly increasing the mobility of the system. Moreover, as above, this was observed for azoSM/VP molar ratios as low as 0.1 for the COOH-functionalized SMs but only for ratios higher than 0.5 for the OH-functionalized SMs. Crystallization has been observed as well in supramolecular systems of P4VP and COOH-functionalized molecules with longer linear alkyl substituents (as tail and/or spacer),[16,48] the linear alkyl chain increasing still more the driving force for crystallization of the small molecule; OH-functionalized molecules with alkyl substituents, in contrast, can be complexed more easily to P4VP up to equimolar proportion,[49] again highlighting the role of acid dimerization as a driving force for crystallization.

It is noteworthy that crystallization has not been reported to date in the existing literature for P4VP-based complexes with hydrogen-bonded azoSMs that are short like in the present azoSM/PDM complexes, whether prepared by spin-coating or solvent-casting (or related techniques involving slow

solvent evaporation), including when using DMF.[26,46] The apparently greater propensity for crystallization in the PDM complexes can be related to the much lower T_g of PDM compared to P4VP, although, as noted above, the T_g's of the azoOH (and, presumably, azoCOOH) complexes with PDM are in a range that is comparable to some similar H-bonded azo complexes based on P4VP (50k).[26,46] This may imply, first of all, that the T_g of a given complex composition may, in fact, be somewhat higher for the P4VP-based analogue than for the PDM-based analogue, thus requiring more solvent evaporation and therefore a longer time, if all other conditions (such as solvent, solution concentration, preparation temperature, drying temperature) are identical, for the latter system to become glassy and thus frozen in. But, even if the T_g's were identical for the two analogous complexes, another reason that may favor crystallization in the PDM- over the P4VP-based complexes is the following. If, as shown above, the T_g of PDM-based complexes increases with azo content and if that of analogous P4VP-based complexes decreases with azo content, then the beginning of phase separation/crystallization actually decreases the degree of complexation, which will result in a decrease in T_g in the PDM complex and an increase in T_g in the P4VP complex. Consequently, further crystallization will be facilitated in the former case (self-accelerating), whereas it will be impeded in the latter case (self-decelerating). It should be added, however, that the T_g dependence on azo content may actually be quite complex and depend also on the intrinsic rigidity of the azo SM used; for example, the T_g may decrease with azo content for low contents due to increasing plasticization and then remain approximately constant or increase with azo content at high content due to increasing effective sidechain density and therefore polymer chain rigidity. This may in part explain the different tendencies noted above regarding the T_g's of different azoSM/P4VP complexes investigated in the literature.

Characterization of the azoSO_3/PDMQ complex. The azoSO_3/PDMQ complex is a simpler system compared to the azoOH and azoCOOH systems. By virtue of its preparation using ion exchange procedures that lead to oppositely charged ionic links with every PDM repeat unit and of the absence of

other detectable ions that could interfere with the azoSO$_3$/PDMQ interactions, there is complete and stable ionic complexation. Structurally, it never shows any sign of crystallization, including when solvent-cast (see Figure S6C). However, it has a liquid crystal structure, notably of the smectic A type where the chromophores form single interdigitated layers, as established previously for this and similar complexes[20] and as indicated in Figure S6C by the amorphous halo at wide angles (in contrast to pure azoSO$_3$ with its many crystalline reflections) and in Figure 4C by the sharp low-angle peak near 2.9º (2θ). This structure is also visible by GIWAXD (Figure S6C). It is worthy of mention that a second-order diffraction peak, not observed in ref. 20, is weakly visible in Figure 4C at twice the angle of the first-order peak, supporting the lamellar (i.e. smectic) structure. DSC shows that this complex has a very high T_g of about 180 ºC (Figure S9), confirming that reported for the lower molecular weight azoSO$_3$/PDMQ complex in ref 20.

The UV-visible spectrum of the azoSO$_3$ complex (Figure 1C) is significantly different from that of the pure azoSO$_3$ in solution, in contrast to the azoOH and azoCOOH systems. This difference can be attributed to excitonic coupling resulting from the smectic A structure in the film. In contrast, the similarity of the film spectra of the azoOH and azoCOOH complexes to their dilute solution spectra, suggests that these complexes are amorphous (isotropic) with no liquid crystal packing.

Surface relief gratings on spin-coated films of the complexes. Two sets of SRG experiments were undertaken. In the first, the azoCOOH and azoOH complexes with different azo:DM molar ratios were compared, using a relatively low laser irradiance (50 mW/cm^2). In the second, the three types of complexes, all at equimolar azo:DM ratios, were compared using a higher laser irradiance (190 mW/cm^2). In all cases, the SRGs were recorded for about 10 min, since the interest of this study was to establish the effect of bonding type and azo content on the polymer mass transport, and clear differences were already apparent under these conditions.

Table 1. Film thicknesses and surface relief grating depths of the spin-coated complexes.

Complex molar ratio	Thickness (nm)	Laser irradiance (mW/cm^2)	Grating depth [a] (nm)
azoOH/PDM			
0.10	202	50	[b]
0.25	227	50	5 (3, [b])
0.50	385	50	17 (12, 9)
0.75	1399	50	26 (22, 20)
1.0	932	50	31 (25, 22)
1.0	210	190	23 [c]
azoCOOH/PDM			
0.10	414	50	1 (1, 1)
0.25	180	50	9 (8, 4)
0.50	238	50	37 (32, 17)
0.75	199	50	45 (39, 25)
1.0	161	50	48 (41, [d])
1.0	177	190	35 [c]
azoSO_3/PDMQ			
1.0	518	50	54 (51, 51)
1.0	590	190	155 [c]

[a] Measured within 2 days of SRG inscription except where otherwise noted (in parenthesis, remeasured 3 and 6 months later). [b] No periodic SRG visible. [c] Measured 3 weeks after SRG inscription. [d] Rough surface obscuring any periodic height variation.

Table 1 lists the thicknesses of the spin-coated films for SRG inscription as well as the average SRG modulation depths measured. Most of the films are about 200±40 nm in thickness, while a few are thicker, particularly the OH complexes of higher azo content due to the higher solution concentrations used (as mentioned in the Experimental section, the azoCOOH is less soluble in DMF than azoOH, and therefore had to be restricted to more dilute solutions). The surface gratings are not expected to be influenced significantly by the differences in film thicknesses as long as they are above about 150 nm and/or well above the grating depths achieved.[50,51] In the present case, the short inscription time of 10

min resulted in grating depths that were always well below the film thicknesses, thus allowing valid comparisons between the materials to be made. Furthermore, the deepest gratings were obtained in the thinnest films, which would not be expected if the effect of film thickness was important.

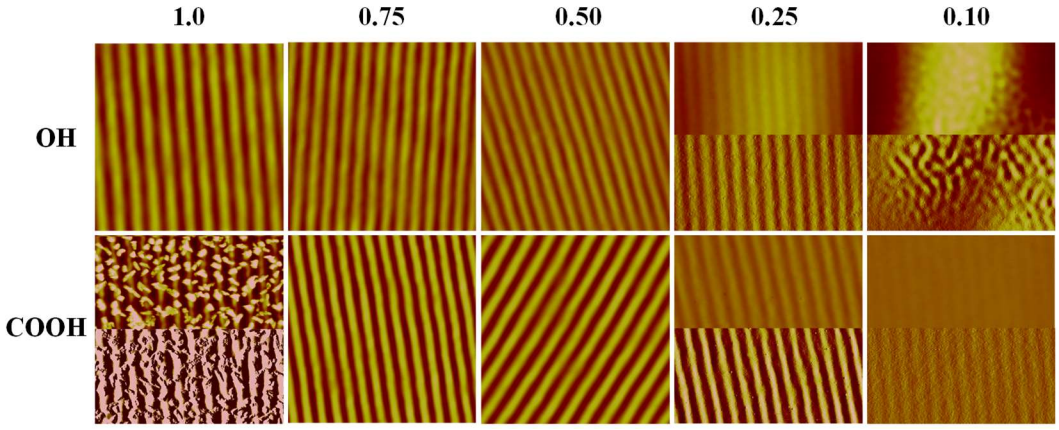

Figure 5. AFM height images (10×10 μm, 100 nm z-scale) of SRGs formed on azoOH/PDM and azoCOOH/PDM complexes at the azo/polymer molar ratios indicated (laser irradiance, 50 mW/cm^2). For azoOH complexes with y=0.25 and 0.10 and azoCOOH complexes with y=1.0, 0.25 and 0.10, composite height (top half) and amplitude (bottom half) images (5×10 μm) are shown.

AFM images of the SRGs for various samples are given in Figure 5 (low irradiance inscription) and Figure S10 (high irradiance inscription). The SRGs are generally smooth, except for azoCOOH/PDM(1.0), which shows considerable roughness superimposed on the SRG that must be related to azoCOOH crystallization, and azoOH/PDM(0.10), which shows a very shallow wavy pattern (most evident in the amplitude image).

The average SRG modulation depths measured from the topographical images (Table 1) can be observed to increase as a function of increasing degree of complexation for both the azoOH and azoCOOH complexes. Furthermore, they are generally higher for the azoCOOH complexes than for the azoOH complexes at any given complexation ratio. However, as shown by the grating depths measured 3 and 6 months after SRG inscription (Table 1), the SRGs tend to slowly self-erase over time, with the

grating depths after 6 mo being about half of those measured initially for the azoCOOH complexes and for the lower molar ratios of the azoOH complexes (the 0.75 and 1.0 molar ratios of the latter appear to be more stable, probably due to their having higher T_g's). SRG self-erasure was also observed for low-T_g all-covalent azo side-chain random copolymers with a polysiloxane backbone.[52] In comparison to the equimolar azoOH and azoCOOH complexes, the SRG for the equimolar azoSO_3 complex film, inscribed at low irradiance, shows a grating depth that is just a little higher than for the equimolar azoCOOH complex. However, for this very high-T_g complex, there is essentially no self-erasure in the six months following inscription. On the other hand, comparison of the depths of the SRGs written on the equimolar films under higher laser irradiance (Table 1) indicates a much higher grating amplitude (4-7x) for the azoSO_3 complex than for the two others, for which the amplitudes are similar or even a little lower than those obtained under lower laser irradiance (this latter result must be related to some degree of self-erasure given that they were AFM-imaged 3 weeks after SRG inscription as well as to some variability in the degree of crystallinity or cristallite sizes in the equimolar azoCOOH and perhaps even azoOH films that is unlikely to be identical in different films of the same sample).

A more direct comparison of the complexes can be obtained from the first-order diffraction efficiencies (DEs), which are averages over larger surfaces and which are measured in situ as the SRGs are being inscribed so that they are not subject to any changes that might occur after inscription. These diffraction efficiencies, recorded as a function of writing time, are given in Figure 6. For the lower laser irradiance, the DE plots are approximately linear over most of the range, and are far from reaching saturation. For the higher laser irradiance, they are approximately linear over the first part of the range and tend towards saturation, particularly for the azoSO_3 complex. Clearly, the saturation values, towards which the latter curves tend, increase in the order, azoSO_3 >> azoCOOH > azoOH.

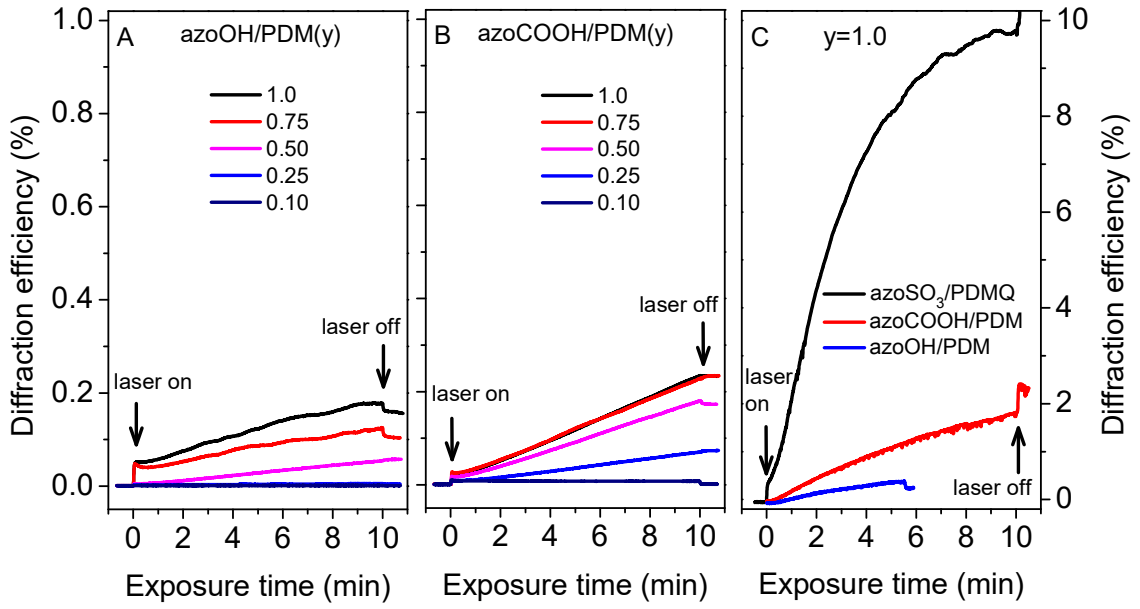

Figure 6. Diffraction efficiency recorded during SRG inscription on the various azo-containing films. A and B: laser irradiance 50 mW/cm^2; C: laser irradiance 190 mW/cm^2. Note that the vertical scale of the rightmost graph is ten times larger than for the two other graphs.

The slopes of the linear portions of the DE curves are plotted in Figure 7 as a function of complexation ratio, y. For SRG inscription at lower irradiance, these values follow the same tendency as the grating depths, notably in their increase as a function of azo content for the azoOH and azoCOOH complexes and in the higher value at each complexation ratio for azoCOOH compared to azoOH. Furthermore, while the increase for the azoOH complexes appears linear from y=0.25 to 1.0, the values for the azoCOOH complexes tend to flatten out for complexation values greater than about 0.5. The latter can be attributed to significant azoCOOH crystallization (consistent with the GIWAXD and POM data), where the crystallized portion cannot participate in the SRG writing process and may even interfere with the process. This crystallization is clearly observed in the AFM image of the SRG for y=1.0 only (Figure 5), probably indicating that any crystallites for y=0.75 are very small and the degree of crystallization too low to be observable by AFM. In contrast, with no or insignificant crystallization in the azoOH films according to the GIWAXD and POM data (infrared suggests that there is some crystallinity in the spin-

coated 1.0 sample, although this may be influenced by the choice of substrate, which was different for IR analysis), the SRG inscription efficiency continues to increase with azo content up to y=1.0. In comparison with the azoOH and azoCOOH complexes, the equimolar azoSO_3 complex gives a still higher DE slope, which (probably coincidentally) appears to be a linear extension of the lower molar ratio (0.1-0.5) azoCOOH complexes.

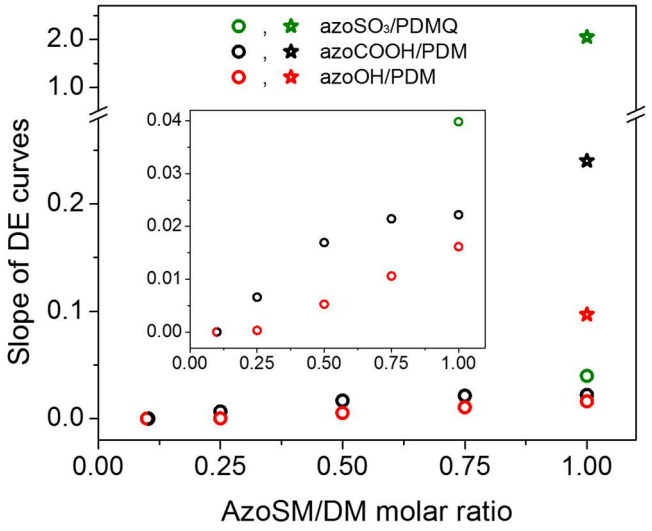

Figure 7. Average slope of the approximately linear portion of the diffraction efficiency (DE) vs. time curves in Figure 6 as a function of the azoSM/DM molar ratio (y). The circles and stars indicate data obtained under lower and higher irradiance, respectively. For better comparison of the lower irradiance radiation data, these are shown with an expanded y-scale in the inset.

Under higher irradiance, the values obtained for inscription of the equimolar complexes is much greater than under lower irradiance. Furthermore, the differences between the (equimolar) samples are also amplified, particularly for the azoSO_3 complex, which is almost 9 times greater than for the azoCOOH complex using higher irradiance compared to less than 2 times greater using lower irradiance (the value for azoCOOH complex, in turn, is about 2.5 times greater than for the azoOH complex under higher irradiance compared to 1.4 times greater under lower irradiance). Overall, the DE data confirm the superior performance of the azoSO_3 complex, as indicated in an earlier study,[20] and show its much

better performance compared to the azoOH and azoCOOH complexes, while the azoCOOH complexes perform somewhat better than the azoOH complexes, and this even at equimolar ratio despite significant crystallization of the azoCOOH in this sample.

It can therefore be concluded that purely ionic complexation is clearly superior to purely hydrogen-bond complexation for efficient SRG inscription in supramolecular polymer systems. This can be related to several factors, the most obvious being the greater strength of the (sulfonate-amine) ionic bond compared to the (phenol-amine) H-bond. There may be a contribution as well from the rigidifying effect of quaternization of the amine moiety, as it was shown in previous work that this is one important factor enhancing SRG efficiency.[20] This increased rigidity and strong complexation is reflected also in the much higher T_g measured for the azoSO_3/PDMQ complex compared to the other two types of complexes. Previous work had shown that SRG efficiency is decreased by an increase in T_g when it is well above the writing temperature,[53] which does not seem to be the case here nor in the (high-T_g) ionic complexes in ref. 20. Possibly, the liquid crystal order in the azoSO_3/PDMQ complex plays a significant role in the high DE despite the high T_g; for example, irradiation possibly causes isomerization of the LC phase due to disruption by the cis isomers[54] and simultaneously decreases the T_g. The overall greater DE for the azoCOOH complexes compared to the azoOH complexes, even in the presence of azoCOOH phase separation/crystallization at the highest molar ratios studied, may also be related to the partially ionic character of the proton transfer complex involved, although simultaneous H-bonding and acid-salt structures obscure drawing a clear correlation.

Importantly, this work also shows that SRGs with relatively good to excellent temporal stability can be written on supramolecular complexes of functionalized azo molecules with PDM despite the intrinsically low T_g of pure PDM. This is possible because complexation increases the T_g of the material to above ambient, which is critical since SRGs are generally not temporally stable in amorphous materials with T_g's near or below ambient temperature[45,52,55]

Finally, it is noteworthy that the molecular weight of the PDM used for the complexes is relatively high, although previous literature concerning all-covalent azo polymers as well as H-bonded supramolecular complexes, including several based on P4VP, indicated that SRG formation efficiency tends to decrease with increase in molecular weight beyond an optimal (oligomeric) range.[2,12,56] A few other examples from the literature similarly indicate efficient SRG formation with high molecular weight systems,[57] including the complex of azoSO_3 with quaternized P4VP.[19,20] The role of molecular weight, which also influences the T_g, is clearly another aspect that requires further investigation in order to draw firmer conclusions regarding structure-property relations for SRG inscription.

In future work, to further understand the effect of supramolecular bond type on SRG formation, it will be of interest to compare the influence of the T_g, by variation of the polymer molecular weight, in a purely ionic complex in parallel with a purely H-bonded complex, complemented by dynamic infrared investigations. Analogous azoSMs that give a liquid crystal structure and an amorphous (i.e. isotropic) structure for a given complex type would help determine how this structure may also play a significant role in SRG formation efficiency.

CONCLUSIONS

A series of analogous azo-containing supramolecular polymer complexes of various azo/polymer molar ratios were prepared with the aim of comparing the nature of the supramolecular bond on SRG formation, notably pure hydrogen bonding using azoOH and PDM, mixed ionic and hydrogen bonding via proton transfer and involving acid-salt structures using azoCOOH and PDM, and pure ionic bonding via ion exchange using azoSO_3 and quaternized PDM (this last at equimolar composition only). It was found that pure ionic bonding is clearly superior in SRG inscription efficiency to the others, while the mixed proton transfer system is somewhat superior to the purely hydrogen-bonded system despite partial azoSM phase separation and crystallization at higher azoSM content for the former. SRG inscription is

possible in these systems in spite of the ambient temperature T_g. Sample preparation was also found to be a critical factor for the azoOH and azoCOOH systems, in that azoSM crystallization can occur relatively easily if the solvent evaporation time is too slow (as in solvent-cast films) or if the drying temperature is too high (near or above the T_g), particularly for azoCOOH due to the contribution of acid dimerization to the driving force for crystallization. This work adds to the increasing body of knowledge and understanding concerning the optical properties of azo-containing materials. It also emphasizes the ease with which different molecular characteristics can be readily modified and compared using the supramolecular strategy, providing a convenient means to deepen understanding of photoresponsive materials.

Acknowledgments. The research was funded by the Natural Sciences and Engineering Research Council (NSERC) of Canada (R.G.S., C.P., C.G.B.), le Fonds de recherche du Québec – Nature et technologies (FRQ-NT) (C.P., C.G.B.), and the Canadian Defence Academy Research Program (CDARP) (R.G.S.). X.W. acknowledges a four-year scholarship through the State-Sponsored Study Abroad Programs (SSSAP) granted by the China Scholarship Council (CSC) as well as start-up funding from Southwest Petroleum University. J.V. acknowledges a FRQ-NT postdoctoral fellowship and funding from the Emil Aaltonen Foundation and Finnish Cultural Foundation. Francine Bélanger and Sylvain Essiembre are specially thanked for their help with the XRD instruments.

Supporting Information. Supplementary NMR, IR, XRD, POM, DSC and AFM data.

REFERENCES

1. Natansohn, A.; Rochon, P. Photoinduced Motions in Azo-Containing Polymers. *Chem. Rev.* **2002,** 102, 4139-4175.

2. Mahimwalla, Z.; Yager, K. G.; Mamiya, J.-i.; Shishido, A.; Priimagi, A.; Barrett, C. J. Azobenzene Photomechanics: Prospects and Potential Applications. *Polym. Bull.* **2012,** 69, 967-1006.

3. Rochon, P.; Batalla, E.; Natansohn, A. Optically Induced Surface Gratings on Azoaromatic Polymer Films. *Appl. Phys. Lett.* **1995,** 66, 136-138.

4. Kumar, J.; Li, L.; Jiang, X. L.; Kim, D.-Y.; Lee, T. S.; Tripathy, S. Gradient Force: The Mechanism for Surface Relief Grating Formation in Azobenzene Functionalized Polymers. *Appl. Phys. Lett.* **1998,** 72, 2096-2098.

5. Kim, D. Y.; Tripathy, S. K.; Li, L.; Kumar, J. Laser-Induced Holographic Surface Relief Gratings on Nonlinear Optical Polymer Films. *Appl. Phys. Lett.* **1995,** 66, 1166-1168.

6. Lee, S.; Kang, H. S.; Park, J.-K. Directional Photofluidization Lithography: Micro/Nanostructural Evolution by Photofluidic Motions of Azobenzene Materials. *Adv. Mater.* **2012,** 24, 2069-2103.

7. Chen, D.; Yoon, J.; Chandra, D.; Crosby, A. J.; Hayward, R. C. Stimuli-Responsive Buckling Mechanics of Polymer Films. *J. Polym. Sci., Part B: Polym. Phys.* **2014,** 52, 1441-1461.

8. Vapaavuori, J.; Laventure, A.; Bazuin, C. G.; Lebel, O.; Pellerin, C. Submolecular Plasticization Induced by Photons in Azobenzene Materials. *J. Am. Chem. Soc.* **2015,** 137, 13510-13517.

9. Yadavalli, N. S.; Loebner, S.; Papke, T.; Sava, E.; Hurduc, N.; Santer, S. A Comparative Study of Photoinduced Deformation in Azobenzene Containing Polymer Films. *Soft Matter* **2016,** 12, 2593-2603.

10. Gao, J.; He, Y.; Liu, F.; Zhang, X.; Wang, Z.; Wang, X. Azobenzene-Containing Supramolecular Side-Chain Polymer Films for Laser-Induced Surface Relief Gratings. *Chem. Mater.* **2007,** 19, 3877-3881.

11. Zettsu, N.; Ogasawara, T.; Mizoshita, N.; Nagano, S.; Seki, T. Photo-Triggered Surface Relief Grating Formation in Supramolecular Liquid Crystalline Polymer Systems with Detachable Azobenzene Unit. *Adv. Mater.* **2008,** 20, 516-521.

12. Priimagi, A.; Lindfors, K.; Kaivola, M.; Rochon, P. Efficient Surface-Relief Gratings in Hydrogen-Bonded Polymer−Azobenzene Complexes. *ACS Appl. Mater. Interfaces* **2009,** 1, 1183-1189.

13. Vapaavuori, J.; Priimagi, A.; Kaivola, M. Photoinduced Surface-Relief Gratings in Films of Supramolecular Polymer-Bisazobenzene Complexes. *J. Mater. Chem.* **2010,** 20, 5260-5264.

14. Koskela, J. E.; Vapaavuori, J.; Hautala, J.; Priimagi, A.; Faul, C. F. J.; Kaivola, M.; Ras, R. H. A. Surface-Relief Gratings and Stable Birefringence Inscribed Using Light of Broad Spectral Range in Supramolecular Polymer-Bisazobenzene Complexes. *J. Phys. Chem. C* **2011,** 116, 2363-2370.
15. Gao, J.; He, Y.; Xu, H.; Song, B.; Zhang, X.; Wang, Z.; Wang, X. Azobenzene-Containing Supramolecular Polymer Films for Laser-Induced Surface Relief Gratings. *Chem. Mater.* **2007,** 19, 14-17.
16. del Barrio, J.; Blasco, E.; Oriol, L.; Alcalá, R.; Sánchez-Somolinos, C. Diblock Copolymer–Azobenzene Complexes Through Hydrogen Bonding: Self-Assembly and Stable Photoinduced Optical Anisotropy. *J. Polym. Sci., Part A: Polym. Chem.* **2013,** 51, 1716-1725.
17. Xiao, S.; Lu, X.; Lu, Q. Photosensitive Polymer from Ionic Self-Assembly of Azobenzene Dye and Poly(Ionic Liquid) and Its Alignment Characteristic toward Liquid Crystal Molecules. *Macromolecules* **2007,** 40, 7944-7950.
18. Kulikovska, O.; Goldenberg, L. M.; Kulikovsky, L.; Stumpe, J. Smart Ionic Sol−Gel-Based Azobenzene Materials for Optical Generation of Microstructures. *Chem. Mater.* **2008,** 20, 3528-3534.
19. Zhang, Q.; Bazuin, C. G.; Barrett, C. J. Simple Spacer-Free Dye-Polyelectrolyte Ionic Complex: Side-Chain Liquid Crystal Order with High and Stable Photoinduced Birefringence. *Chem. Mater.* **2008,** 20, 29-31.
20. Zhang, Q.; Wang, X.; Barrett, C. J.; Bazuin, C. G. Spacer-Free Ionic Dye-Polyelectrolyte Complexes: Influence of Molecular Structure on Liquid Crystal Order and Photoinduced Motion. *Chem. Mater.* **2009,** 21, 3216-3227.
21. Ahmed, R.; Priimagi, A.; Faul, C. F. J.; Manners, I. Redox-Active, Organometallic Surface-Relief Gratings from Azobenzene-Containing Polyferrocenylsilane Block Copolymers. *Adv. Mater.* **2012,** 24, 926-931.
22. Koskela, J. E.; Liljeström, V.; Lim, J.; Simanek, E. E.; Ras, R. H. A.; Priimagi, A.; Kostiainen, M. A. Light-Fuelled Transport of Large Dendrimers and Proteins. *J. Am. Chem. Soc.* **2014,** 136, 6850-6853.
23. Priimagi, A.; Cavallo, G.; Forni, A.; Gorynsztejn–Leben, M.; Kaivola, M.; Metrangolo, P.; Milani, R.; Shishido, A.; Pilati, T.; Resnati, G.; Terraneo, G. Halogen Bonding versus Hydrogen Bonding in Driving Self-Assembly and Performance of Light-Responsive Supramolecular Polymers. *Adv. Funct. Mater.* **2012,** 22, 2572-2579.
24. Saccone, M.; Dichiarante, V.; Forni, A.; Goulet-Hanssens, A.; Cavallo, G.; Vapaavuori, J.; Terraneo, G.; Barrett, C. J.; Resnati, G.; Metrangolo, P.; Priimagi, A. Supramolecular Hierarchy

Among Halogen and Hydrogen Bond Donors in Light-Induced Surface Patterning. *J. Mater. Chem. C* **2015,** 3, 759-768.

25. Vapaavuori, J.; Heikkinen, I. T. S.; Dichiarante, V.; Resnati, G.; Metrangolo, P.; Sabat, R. G.; Bazuin, C. G.; Priimagi, A.; Pellerin, C. Photomechanical Energy Transfer to Photopassive Polymers through Hydrogen and Halogen Bonds. *Macromolecules* **2015,** 48, 7535-7542.

26. Vapaavuori, J.; Valtavirta, V.; Alasaarela, T.; Mamiya, J.-I.; Priimagi, A.; Shishido, A.; Kaivola, M. Efficient Surface Structuring and Photoalignment of Supramolecular Polymer–Azobenzene Complexes through Rational Chromophore Design. *J. Mater. Chem.* **2011,** 21, 15437-15441.

27. Schab-Balcerzak, E.; Sobolewska, A.; Stumpe, J.; Hamryszak, L.; Bujak, P. Surface Relief Gratings in Azobenzene Supramolecular Systems Based on Polyimides. *Opt. Mater.* **2012,** 35, 155-167.

28. Kryuchkov, M. A.; Detrembleur, C.; Jérôme, R.; Prud'homme, R. E.; Bazuin, C. G. Synthesis and Thermal Properties of Linear Amphiphilic Diblock Copolymers of L-Lactide and 2-Dimethylaminoethyl Methacrylate. *Macromolecules* **2011,** 44, 5209-5217.

29. Zhang, X.; Xia, J.; Matyjaszewski, K. Controlled/"Living" Radical Polymerization of 2-(Dimethylamino)ethyl Methacrylate. *Macromolecules* **1998,** 31, 5167-5169.

30. Xia, J. H.; Zhang, X.; Matyjaszewski, K. Atom Transfer Radical Polymerization of 4-Vinylpyridine. *Macromolecules* **1999,** 32, 3531-3533.

31. Zhang, L.; Cole, J. M.; Dai, C. Variation in Optoelectronic Properties of Azo Dye-Sensitized TiO_2 Semiconductor Interfaces with Different Adsorption Anchors: Carboxylate, Sulfonate, Hydroxyl and Pyridyl Groups. *ACS Appl. Mater. Interfaces* **2014,** 6, 7535-7546.

32. Karukstis, K. K.; Savin, D. A.; Loftus, C. T.; D'Angelo, N. D. Spectroscopic Studies of the Interaction of Methyl Orange with Cationic Alkyltrimethylammonium Bromide Surfactants. *J. Colloid Interf. Sci.* **1998,** 203, 157-163.

33. Priimagi, A.; Cattaneo, S.; Ras, R. H. A.; Valkama, S.; Ikkala, O.; Kauranen, M. Polymer−Dye Complexes: A Facile Method for High Doping Level and Aggregation Control of Dye Molecules. *Chem. Mater.* **2005,** 17, 5798-5802.

34. Priimagi, A.; Kaivola, M.; Rodriguez, F. J.; Kauranen, M. Enhanced Photoinduced Birefringence in Polymer-Dye Complexes: Hydrogen Bonding Makes a Difference. *Appl. Phys. Lett.* **2007,** 90, 121103.

35. TCI America Safety Data Sheet. https://www.spectrumchemical.com/MSDS/TCI-H0237.pdf (accessed Mar. 31, 2016).

36. van de Wetering, P.; Moret, E. E.; Schuurmans-Nieuwenbroek, N. M. E.; van Steenbergen, M. J.; Hennink, W. E. Structure−Activity Relationships of Water-Soluble Cationic Methacrylate/Methacrylamide Polymers for Nonviral Gene Delivery. *Bioconjugate Chem.* **1999,** 10, 589-597.

37. Brozoski, B. A.; Coleman, M. M.; Painter, P. C. Local Structures in Ionomer Multiplets. A Vibrational Spectroscopic Analysis. *Macromolecules* **1984,** 17, 230-234.

38. Brandys, F. A.; Masson, P.; Guillon, D.; Bazuin, C. G. Ionically Grafted Side-Chain Polymers: Blends of an Acid-Functionalized Mesogen with Poly(ethylene imine). *Macromol. Chem. Phys.* **2001,** 202, 856-865.

39. Speakman, J. C. Acid Salts of Carboxylic Acids, Crystals with Some 'Very Short' Hydrogen Bonds. *Struct. Bond.* **1972,** 12, 141-199.

40. Lindemann, R.; Zundel, G. Polarizability, Proton Transfer and Symmetry of Energy Surfaces of Carboxylic Acid-N-Base Hydrogen Bonds. Infrared Investigations. *J. Chem. Soc., Faraday Trans. II* **1977,** 73, 788-803.

41. Coleman, M. M.; Lee, J. Y.; Painter, P. C. Acid Salts and the Structure of Ionomers. *Macromolecules* **1990,** 23, 2339-2345.

42. Tork, A.; Bazuin, C. G. Mixtures of Tertiary Amine-Functionalized Mesogens with Poly(acrylic acid). *Macromolecules* **2001,** 34, 7699-7706.

43. Bazuin, C. G.; Boivin, J.; Tork, A.; Tremblay, H.; Bravo-Grimaldo, E. Variable Composition Mixtures of a Tertiary Amine-Functionalized Mesogen and Poly(acrylic acid). *Macromolecules* **2002,** 35, 6893-6899.

44. Kornienko, E. V.; Sycheva, T. I.; Kuptsov, S. A.; Bezborodov, V. S.; Lebedeva, T. L.; Tal'roze, R. V.; Plate, N. A. Structuration in Solutions of β-N-Dimethylamino-4-Dodecyloxypropiophenone Salts and its Complexes with Polyacrylic Acid. *Polym. Sci.* **1992,** 34, 997-1000.

45. Vapaavuori, J.; Ras, R. H. A.; Kaivola, M.; Bazuin, C. G.; Priimagi, A. From Partial to Complete Optical Erasure of Azobenzene-Polymer Gratings: Effect of Molecular Weight. *J. Mater. Chem. C* **2015,** 3, 11011-11016.

46. Priimagi, A.; Vapaavuori, J.; Rodriguez, F. J.; Faul, C. F. J.; Heino, M. T.; Ikkala, O.; Kauranen, M.; Kaivola, M. Hydrogen-Bonded Polymer−Azobenzene Complexes: Enhanced Photoinduced Birefringence with High Temporal Stability through Interplay of Intermolecular Interactions. *Chem. Mater.* **2008,** 20, 6358-6363.

47. Wu, S.; Bubeck, C. Macro- and Microphase Separation in Block Copolymer Supramolecular Assemblies Induced by Solvent Annealing. *Macromolecules* **2013,** 46, 3512-3518.
48. Brandys, F. A.; Bazuin, C. G. Mixtures of an Acid-Functionalized Mesogen with Poly(4-vinylpyridine). *Chem. Mater.* **1996,** 8, 83-92.
49. de Wit, J.; van Ekenstein, G. A.; Polushkin, E.; Kvashnina, K.; Bras, W.; Ikkala, O.; ten Brinke, G. Self-Assembled Poly(4-vinylpyridine)−Surfactant Systems Using Alkyl and Alkoxy Phenylazophenols. *Macromolecules* **2008,** 41, 4200-4204.
50. Kim, D. Y.; Li, L.; Jiang, X. L.; Shivshankar, V.; Kumar, J.; Tripathy, S. K. Polarized Laser Induced Holographic Surface Relief Gratings on Polymer Films. *Macromolecules* **1995,** 28, 8835-8839.
51. Fukuda, T.; Matsuda, H.; Shiraga, T.; Kimura, T.; Kato, M.; Viswanathan, N. K.; Kumar, J.; Tripathy, S. K. Photofabrication of Surface Relief Grating on Films of Azobenzene Polymer with Different Dye Functionalization. *Macromolecules* **2000,** 33, 4220-4225.
52. Luca, A. R.; Moleavin, I.-A.; Hurduc, N.; Hamel, M.; Rocha, L. Mass Transport in Low Tg Azo-Polymers: Effect on the Surface Relief Grating Induction and Stability of Additional Side Chain Groups Able to Generate Physical Interactions. *Appl. Surf. Sci.* **2014,** 290, 172-179.
53. Börger, V.; Pohle, S.; Kuliskovska, O.; Gharaggozloo-Hubmann, K.; Stumpe, J.; Menzel, H. Azobenzene-Containing Polymers for Surface Relief Gratings. *Macromol. Symp.* **2009,** 275–276, 257-265.
54. Zhang, Q.; Bazuin, C. G. Solvent Manipulation of Liquid Crystal Order and Other Properties in Azo-Containing Surfactomesogen/Poly(styrene sulfonate) Complexes. *Macromol. Chem. Phys.* **2010,** 211, 1071-1082.
55. Viswanathan, N. K.; Kim, D. Y.; Bian, S.; Williams, J.; Liu, W.; Li, L.; Samuelson, L.; Kumar, J.; Tripathy, S. K. Surface Relief Structures on Azo Polymer Films. *J. Mater. Chem.* **1999,** 9, 1941-1955.
56. Barrett, C. J.; Natansohn, A. L.; Rochon, P. L. Mechanism of Optically Inscribed High-Efficiency Diffraction Gratings in Azo Polymer Films. *J. Phys. Chem.* **1996,** 100, 8836-8842.
57. Yang, S.; Li, L.; Cholli, A. L.; Kumar, J.; Tripathy, S. K. Photoinduced Surface Relief Gratings on Azocellulose Films. *J. Macromol. Sci., A* **2001,** 38, 1345-1354.